

## Synthesis of Ag doped ZnO nanoparticles using *Datura metel* L. leaf extract and their prospect for novel application to enhance shelf life of selected fruits and vegetables

U.S. Senapati<sup>a,\*</sup>, T. Kataki<sup>b</sup>, H. Kalita<sup>b</sup>

<sup>a</sup>*Department of Physics, Handique Girls' College, Guwahati-781001, Assam, India*

<sup>b</sup>*Advanced Level Institutional Biotech Hub, Handique Girls' College, Guwahati-781001, Assam, India*

This work presents a unique method for synthesizing silver (Ag) doped zinc oxide (ZnO) NPs using *Datura metel* L. leaf extract as capping and reducing agents. The formation of Ag doped ZnO NPs was validated by XRD, EDAX, TEM and HRTEM analysis. FESEM was used to analyze the morphology of the Ag doped ZnO NPs and FTIR was utilized to detect the different functional groups contained in the extract of *Datura metel* L. leaf. The Ag doped ZnO NPs showed antibacterial activity against Gram-positive and Gram-negative bacteria isolated from spoiled fruits and vegetables. The antimicrobial susceptibility of Ag doped ZnO NPs against the isolates were in correlation to the standard antibiotics. Therefore, this green synthesized Ag doped ZnO NPs can be utilized as antibiotic substitutes to prevent microbial contamination of fruits and vegetables and extend their shelf life.

(Received December 21, 2024; Accepted May 6, 2025)

*Keywords:* Ag doped ZnO NPs, Green synthesis, XRD, antimicrobial activity, Shelf life

### 1. Introduction

Nutrients and bioactive substances that are beneficial for human health can be found in fresh fruits and vegetables. Nevertheless, these products have a limited post-harvest life and are extremely perishable, resulting in large losses globally. Microorganisms that can cause diseases in humans can also contaminate fruits and vegetables. Due to inadequate storage facilities and inadequate transportation, post-harvest losses caused by microbes are most prevalent in underdeveloped nations [1, 2]. To offset these losses, excessive pesticide treatment has occurred both before and after harvest [3]. In addition, consumers are cautious of eating fruits and vegetables that have been chemically treated because of the unanticipated health risks they pose [4]. More than 40% of fruits and vegetables are lost after harvest worldwide, demonstrating the insufficiency of current methods to minimize this loss and the necessity of developing strict guidelines that are safe for consumers as well as cost-effective for growers or traders. Researchers are focusing their efforts on a variety of techniques, such as nano-based products and approaches to increase the shelf life of fruits and vegetables, in order to provide the next generation of environmentally friendly solutions.

Nanotechnology has emerged as an option for the development of new technologies to extend the shelf life of fruits and vegetables in recent years. Its submicron size affords a novel approach to enhancing the functionalities of materials for food preservation, including gas exchange, mechanical and optical characteristics, water barrier, and increased sensitivity to antioxidant and antibacterial activity [5]. Zinc oxide (ZnO), an n-type semiconductor belonging to the II-VI semiconductor oxide family, with a broad band gap of around 3.37 eV. Its structure is hexagonal, and each zinc ion is surrounded by four oxygen ions in a tetrahedral coordination, and vice versa. As a result, they could be used in gas sensors, photovoltaics, optical coatings, and photocatalysts [6]. Because of its low cytotoxicity, selectivity, and heat tolerance, zinc oxide is also a promising antibacterial agent. By targeting bacterial sulfhydryl groups, it prevents the functioning of glycolytic enzymes. ZnO is a promising choice due to the aforementioned characteristics, but a few

---

\* Corresponding author: [udaysankargu@gmail.com](mailto:udaysankargu@gmail.com)

<https://doi.org/10.15251/JOBM.2025.172.61>

disadvantages, including a high optical band gap, a higher electron-hole pair recombination rate, and the production of less reactive oxygen species, prevent ZnO from being used for longer. Doping, particularly with noble metals, is one of the methods that researchers have tried to increase its efficiency [7]. Silver (Ag) is the most promising material for doping because of its excellent stability. It has antibacterial and antioxidant properties as well. Because of its inherent antimicrobial properties and surface plasmon effect in visible regions, silver is the noble metal that draws the most attention. Photogenerated electron and hole pairs have a longer recombination lifetime when silver atoms are doped. It also improves the material's optical band gap. By doping the Ag atoms with ZnO nanoparticles, the window for other uses is so opened.

The varied agro climatic conditions in northeastern India support the cultivation of a wide range of tropical, sub-tropical, and temperate fruits and vegetables that are enhanced with high levels of fiber and nutrients. Because it diversifies the agriculture sector, which is crucial for generating long-term revenue and job possibilities, horticulture offers enormous potential for the expansion and development of the mainly agricultural region. Many fruits and vegetables grown in the northeast produce a viable surplus that can be marketed both domestically and internationally. In India, brinjal (*Solanum melongena* L.) is a widely consumed vegetable. In Assam, brinjal is grown on 17,760 hectares, yielding 2, 86,350 metric tons annually [8]. In Northeast India, chili (*Capsicum annum* L.) is one of the most essential vegetables, helping farmers grow economically [9]. Approximately 20,189 tons of green chilies are grown in Assam on 20,459 hectares of land. Around the world, bananas (*Musa paradisiaca* L.) are considered to be one of the main fruit crops. Assam is responsible for 2.4% of India's total banana production [10]. Because they are a nutrient-dense part of a well-balanced diet and include a variety of health-promoting components, tomatoes (*Solanum lycopersicum* L.) are the most important fruit [11]. Every year, Assam produces almost 396.024 thousand metric tons of tomatoes [12].

This study utilized *Datura metel* L., a medicinal plant that is readily available in the locality, to green synthesis Ag-doped ZnO NPs. As far as we have found, there are no report on the production of Ag-doped ZnO NPs using *Datura metel* L. Thus, the goal of this study was to use *Datura metel* L. to add another dimension to the environmentally friendly synthesis of Ag-doped ZnO NPs. Additionally, the antibacterial activity of produced Ag-doped ZnO NPs against spoilage microorganisms isolated from locally accessible vegetables (Chili and brinjal) and fruits (banana and tomato) was investigated.

## 2. Materials and methods

### 2.1. Experimental materials

This study used leaf extract from *Datura metel* L., sodium hydroxide [NaOH], silver nitrate ( $\text{AgNO}_3$ ), and zinc acetate dehydrate [ $\text{Zn}(\text{CH}_3\text{COO})_2 \cdot 2\text{H}_2\text{O}$ ]. The chemicals and glassware were provided by Sigma Aldrich, India. Leaves of *Datura metel* L. were collected from a neighboring forest in Guwahati, Assam, India, and a herbalist authenticated their identity.

### 2.2. Preparation of *Datura metel* L. leaf extract

To remove undesirable contaminants, the *Datura metel* L. were rinsed with distilled water. 20 g *Datura metel* L. leaf was cooked in 100 ml distilled water for 20 min and then filtered with filter paper (Whatman No.1). The filtrate was cooled to room temperature. The resulting filtrate was the extract of *Datura metel* L. leaf.

### 2.3. Methods

#### 2.3.1. Synthesis of Ag-doped ZnO nanoparticles

The leaf extract from *Datura metel* L. was added drop by drop to a solution of Zn ( $\text{CH}_3\text{COO}$ )<sub>2</sub> · 2H<sub>2</sub>O (0.5 M), and then AgNO<sub>3</sub> (0.005M) was added. The pH of the mixture was adjusted to 12 by adding NaOH solution. Ag doped ZnO nano colloid was produced by stirring the resultant mixture for approximately 2 h in a magnetic stirrer and then allowing it stay at room temperature overnight to finish the reaction. The amount of *Datura metel* L. leaf extract was varied for 10 ml, 20 ml, 30 ml, and 40 ml in order to investigate the role it plays as capping and reducing

agents in the production of Ag doped ZnO nanoparticles. The precipitate was removed from the reaction solution by centrifugation at 2,000 rpm for 15 min. Before being crushed into a fine powder, the final product was dried for 48 h in a hot air oven set at 80°C. The four final products had the names A, B, C, and D. A schematic diagram for the green production of Ag-doped ZnO nanoparticles is shown in Figure 1.

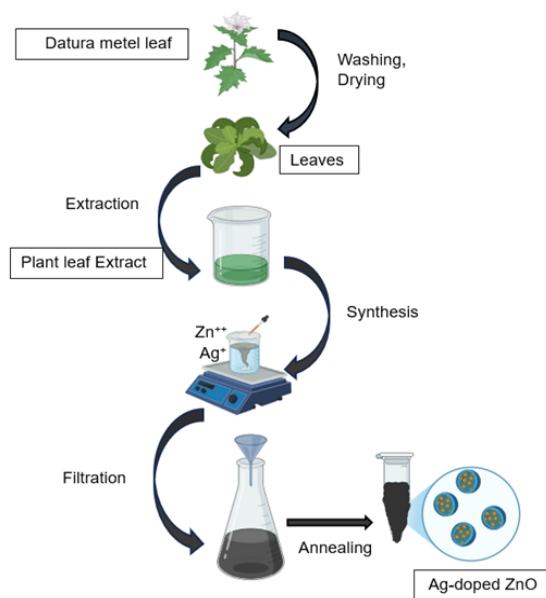


Fig.1. Schematic diagram for green synthesis of Ag doped ZnO nanoparticles.

### 2.3.2. Characterization of Ag doped ZnO nanoparticles

An X-ray diffractometer (Philips X' pert with CuK $\alpha$  radiation) with a wavelength of 0.154 nm was used to record X-ray diffraction patterns. A JEOL JEM 2100 was used to take TEM micrographs. JEOL JES-FA200 was used to take FESEM micrographs. The EDAX (Oxford, INCA-7587) was used to analyze the elemental analysis and purity of the samples. The FTIR spectra were recorded using a Perkin Elmer spectrum RXI FTIR instrument.

### 2.3.3. Sample collection

Samples of fruit and vegetables were collected from a nearby market in sterile polythene bags and brought to the lab. Two fruits (banana and tomato) and two vegetables (brinjal and chili) had been selected as samples for microbial isolation [13].

### 2.3.4. Isolation of microorganisms

The procedure described by Hasan et al. [14] was used to isolate the bacteria with a few minor modifications. One gram of the spoiled tomato part was cut using a sterile blade and put in a sterile test tube with 9 ml of distilled water to make the stock solution for the tomato sample. The sample was completely crushed using a sterile glass rod. 50  $\mu$ l of each dilution was then applied to nutrient agar (NA) plates using a sterile L-shaped spreader after the suspension had been serially diluted from  $10^1$  to  $10^7$  dilutions. The plates were then incubated for 24 h at 37°C. The remaining samples underwent the same procedure.

### 2.3.5. Microbial identification

The microbial isolates were selected and sub cultured to make pure cultures based on the morphologies of their colonies. They were also grown on MacConkey agar plates and maintained on NA slants. The cellular morphology of the microorganisms was investigated using Gram staining.

To provide a more precise identification of the bacteria, the isolates underwent bioinformatics analysis and 16S rRNA sequencing[15].

### **2.3.6. Antimicrobial susceptibility testing**

Using the Kirby-Bauer disk diffusion method, the bacterial isolates' in vitro antimicrobial susceptibility to six standard antibiotics - nitrofurantoin [NIT], vancomycin [VA], amoxicillin and clavulanic acid [AMC], gentamicin [GEN], ciprofloxacin [CIP], and erythromycin [E] was determined prior to evaluating how effectively Ag-doped ZnO nanoparticles performed against the isolates. Standardized suspensions of the isolates were made with peptone water and cultivated at 37°C for two to six hours. A lawn was made on Mueller Hinton agar after the turbidity was brought down to 0.5 McFarland standards. After repeating the process with the remaining isolates that were selected, the plates were incubated at 37°C for 24 h. The diameter of the clear zones formed were measured and recorded [16][17].

### **2.3.7. Well diffusion method**

The agar-well diffusion method was used to assess the produced Ag-doped ZnO nanoparticles' in vitro antibacterial efficacy against the isolates. The Kirby-Bauer disk diffusion method was followed to create standardized suspensions of the isolates. After adjusting the suspension's turbidity to 0.5 McFarland standards, a lawn was made using the adjusted bacterial suspension on Mueller Hinton agar. Wells measuring 6 mm in diameter were made on the plates using sterile micropipette tips and the wells were filled with 50 µl of various extract concentrations of biosynthesized Ag-doped ZnO nanoparticles at the concentration of 20 mg/L. At 37°C, the plates were incubated overnight. Any resultant clear area surrounding the wells was noted [18].

### **2.3.8. Determination of minimum inhibitory concentration (MIC)**

The MIC of Ag-doped ZnO NPs synthesized by using different concentrations of *Datura metel* L. leaf extract (10ml and 40ml) was determined against the selected bacterial isolates by the broth microdilution method. A bacterial suspension was prepared by inoculating 3-4 colonies from the NA plates in sterile saline and a turbidity equivalent to 0.5 McFarland standards was achieved. The suspension was further diluted to obtain a concentration of approximately  $1.0 \times 10^6$  CFU/mL by inoculating 1mL of inoculum to 20 mL of Mueller Hinton broth. A serial two-fold dilution of the Ag-doped ZnO nanoparticles (for each variant) in concentration ranging from 100 mg/L to 10 mg/L was used. 200 µl of Ag-doped ZnO nanoparticle sample was added to the wells of the first column of a 96-well plate. 100 µl of Mueller Hinton broth was then added to all the remaining wells and 100 µl of Ag-doped ZnO nanoparticle solution was transferred from the first well to the next well using a micropipette to achieve a 1:2 dilution, another 100 µl was then transferred from the second well to the next resulting in a 1:4 dilution. This step was repeated for each Ag-doped ZnO nanoparticle variant up to the ninth dilution. Following this 10 µl of previously prepared bacterial suspension was added to each well. The procedure was repeated for each bacterial isolate. Additionally, a growth control and a negative control were added to each plate. The plates were incubated at 37°C for 24 ± 2hrs. Following incubation, the microtiter plates were observed for visible growth. Furthermore, 1X resazurin was prepared and 10 µl of resazurin solution was added to the well and incubated for additional 2-4 hrs. The color change was recorded. The lowest concentration of Ag-doped ZnO nanoparticle at which no color change was observed was taken as the MIC [14].

## **3. Results and discussion**

### **3.1. XRD study**

XRD patterns of Ag-doped ZnO nanoparticles synthesized by using leaf extract of *Datura metel* L. are displayed in Figure 2. According to JCPDS card no. 36-1451, the diffraction peaks found at 2θ values of 31.97°, 34.69°, 36.55°, 47.69°, 56.86°, 63.17°, 66.63°, 68.25°, and 69.35° might be attributed to the (100), (002), (101), (102), (110), (103), (200), (112), and (201) planes of ZnO with hexagonal wurtzite structure, respectively. Other peaks were found at 2θ values of 38.40°, 44.59°, and 64.77°, which correspond to the Ag's (111), (200), and (220) planes, respectively [19]. They matched the Ag nanoparticles' face-centered cubic shape (JCPDS card no.04-0783). The

successfully produced Ag-doped ZnO nanoparticles employing *Datura metel* L. leaf extract was confirmed by the absence of any impurity peaks.

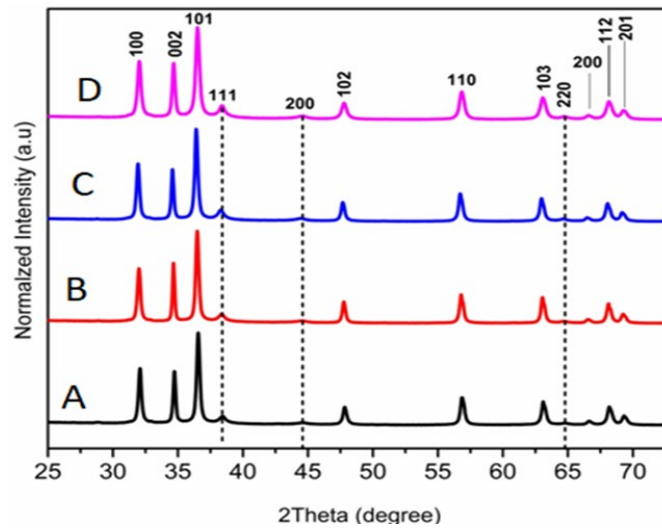


Fig. 2. XRD patterns of Ag doped ZnO nanoparticles.

The crystallite size ( $D$ ) and d-spacing were calculated using the conventional formulas,

$$D = \frac{k\lambda}{\beta \cos\theta} \text{ (Debye Scherrer formula)} \quad (1)$$

and

$$d = \frac{\lambda}{2 \sin\theta} \quad (2)$$

where  $D$  is the average crystallite size,  $\lambda$  is the incident beam's wavelength,  $k$  is the form factor, which has a value of 0.89,  $\beta$  is the full width of the half maximum peak value, and  $\theta$  is the Bragg's angle. Zn with the same ionic radius ( $0.89\text{\AA}$  and  $0.88\text{\AA}$ , respectively) replaced the position of Ag. Additionally, the lattice parameters for the specimens along with the volume were also calculated for the hexagonal wurtzite ZnO using the equations  $\frac{1}{d^2} = \frac{4(h^2+hk+k^2)}{3a^2} + \frac{l^2}{c^2}$  and  $V = \frac{\sqrt{3}}{2} a^2 c$ , where  $\langle hkl \rangle$  represents the Miller indices of a plane and  $d$  is the interplanar spacing between the planes,  $a$  and  $c$  are the lattice parameters

Table.1. Structural parameters of Ag doped ZnO NPs.

Sample	Lattice parameters							
	FWHM (rad)	Peak positions ( $^{\circ}$ )	Crystalline size (nm)	a ( $\text{\AA}$ )	c ( $\text{\AA}$ )	c/a	d ( $\text{\AA}$ )	Unit cell Volume ( $\text{\AA}^3$ )
A	0.0065	101	22	3.396	4.897	1.442	2.45	49.13
B	0.0056	101	26	3.398	4.899	1.441	2.47	49.04
C	0.0053	101	27	3.402	4.910	1.443	2.50	49.27
D	0.0054	101	28	3.407	4.912	1.442	2.53	49.43

From table 1, it was found that as the extract volume increased, the samples' crystallite sizes also increased. With 10 ml of extract, the size was 22 nm; with 40 ml of extract, the size increased significantly to 28 nm. It indicated that the 10 ml extract volume with the smallest size of 22 nm was the ideal extract volume. However, it also showed that a higher extract volume might raise the probability of particle agglomeration [20]. A 10 ml extract volume could provide enough antioxidants to produce Ag-doped ZnO NPs that was lower in size; however, if there was too much extract present, the process might persist and the size could increase [21]. The average lattice parameters for Ag doped ZnO were  $a = b = 3.40075 \text{ \AA}$ ,  $c = 4.9045 \text{ \AA}$ , and  $c/a = 1.442$  (Table 1). These values were consistent with the JCPDS file no. 36-1451 ( $a = b = 3.25350 \text{ \AA}$ ,  $c = 5.21510 \text{ \AA}$ , and  $c/a = 1.602$ ). Additionally, it was found that the d-spacing increased from 2.45 to 2.53  $\text{\AA}$  when the crystallite size increased monotonically from 22 nm (sample A) to 28 nm (sample D). Furthermore, it was found that the lattice volumes exceeded the ICDD threshold value (47.620  $\text{\AA}$ ).

### 3.2. FESEM and EDAX study

Figure 3 shows the morphology of the green synthesized Ag-doped ZnO NPs employing varying amounts of leaf extract from *Datura metel* L. Using 10 ml of *Datura metel* L. leaf extract, Ag-doped ZnO NPs were produced, resulting in an agglomerated spherical structure (Fig. 3(a)). Figures 3(b), (c), and (d) correspondingly depict the Ag-doped ZnO NPs synthesized with 20, 30, and 40 ml of *Datura metel* L. leaf extract; an agglomerated flake-like structure was produced. The volume of *Datura metel* L. leaf extract thus played a significant effect in the morphology of the Ag doped ZnO NPs, as was revealed from the FESEM images.

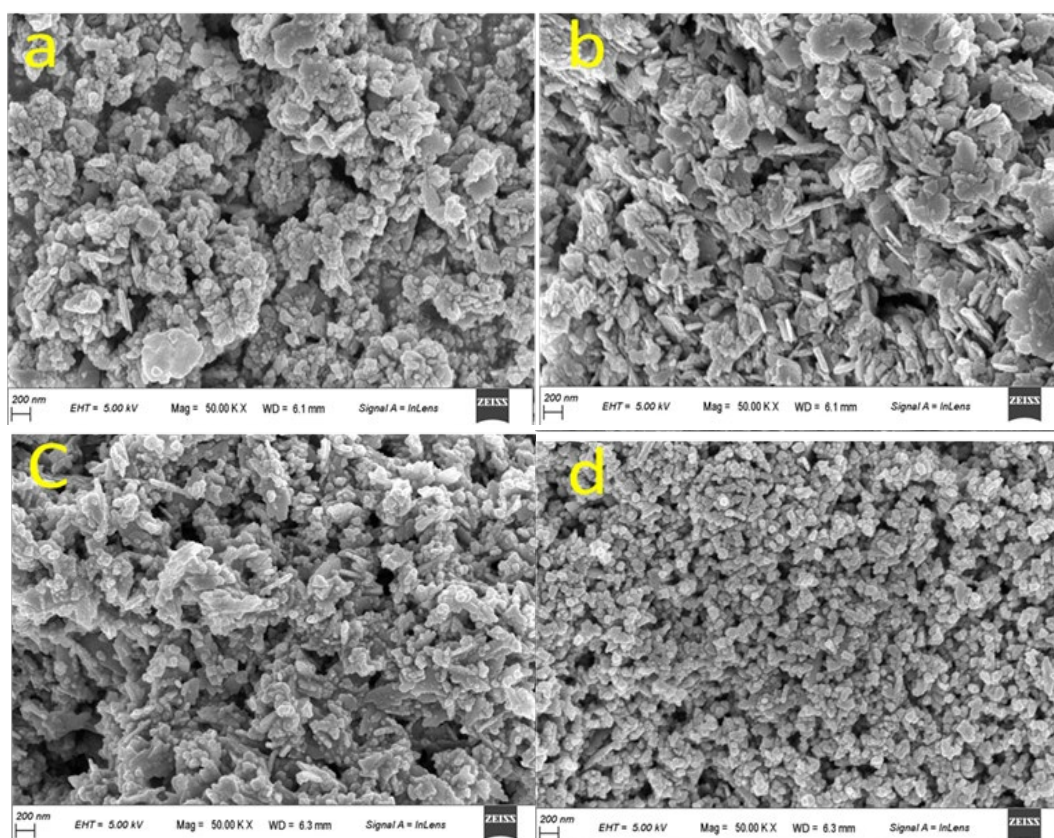


Fig.3. FESEM images of Ag doped ZnO nanoparticles.

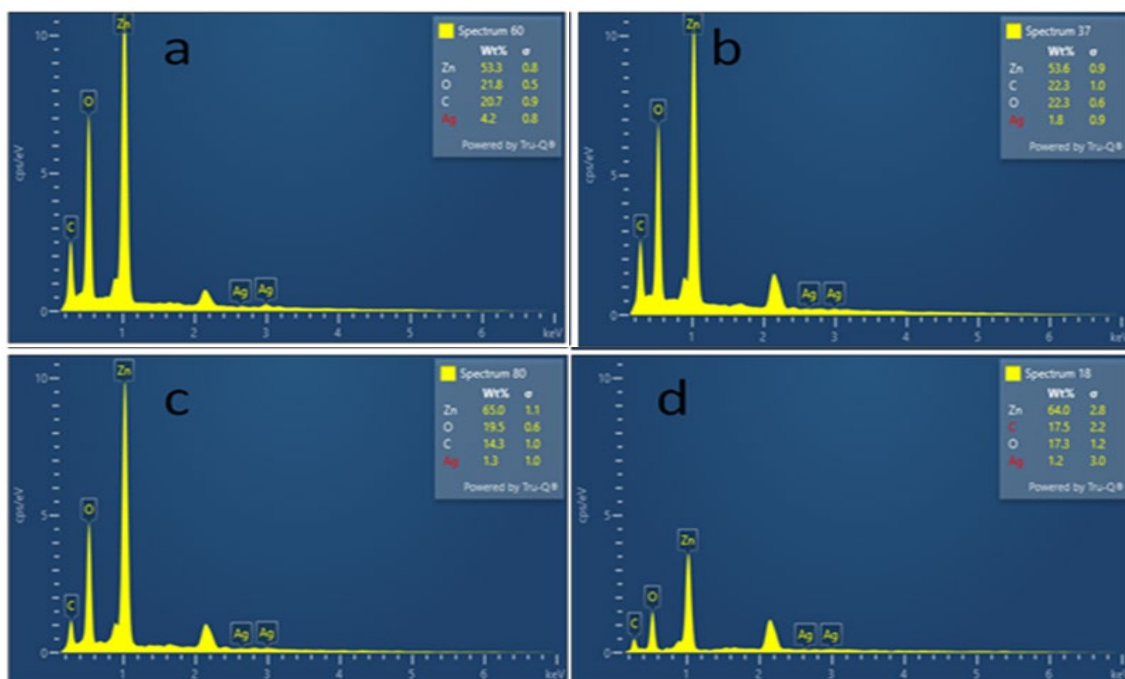


Fig. 4. EDAX spectra of Ag doped ZnO nanoparticles.

The synthesized Ag doped ZnO NPs were confirmed to include O, Zn, and Ag by elemental analysis performed by EDAX (Fig. 4). Thus, it was evident from the EDAX study that Ag was doped into ZnO. The additional signal of C was found due to the biomolecules present in *Datura metel* L. leaf extract. The insets in Figure 4 illustrate the elements' weight and atomic percentages in the prepared samples.

### 3.3. TEM and HRTEM study

The TEM images of Ag-doped ZnO NPs synthesized with 10 ml and 40 ml of *Datura metel* L. leaf extract are displayed in Figure 5(a) and (b), respectively. Figure 5(a) shows spherical and agglomerated particles at the lowest concentration of the extract (sample A), while Figure 5(b) shows rod-shaped particles at the highest concentration of the extract (sample D). According to TEM analysis, the shape of Ag-doped ZnO NPs varied as the extract volume increased, and these changes were consistent with the findings of FESEM. It was found that the spherical particles' average size was around 20 nm (Fig. 6(b)). The length and width of a single rod-shaped particle were also seen to be approximately 230 and 52 nm, respectively (Fig. 5(b)).

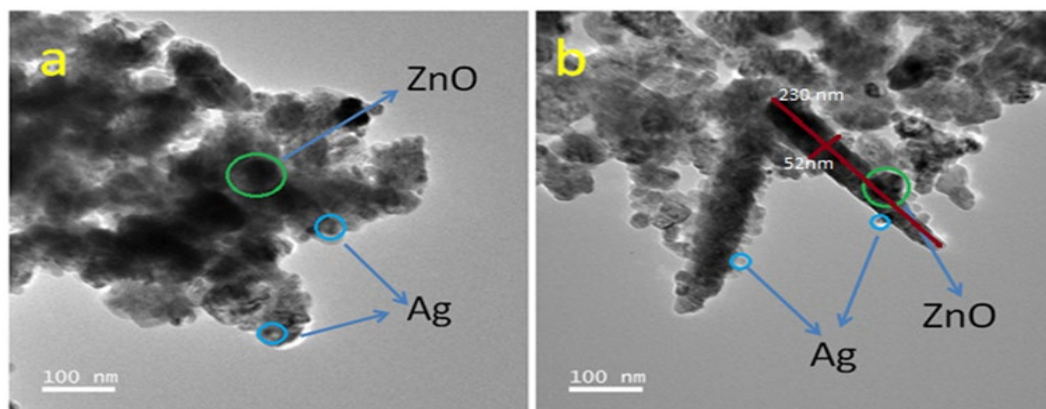


Fig. 5. TEM image of (a) sample A and (b) sample D.

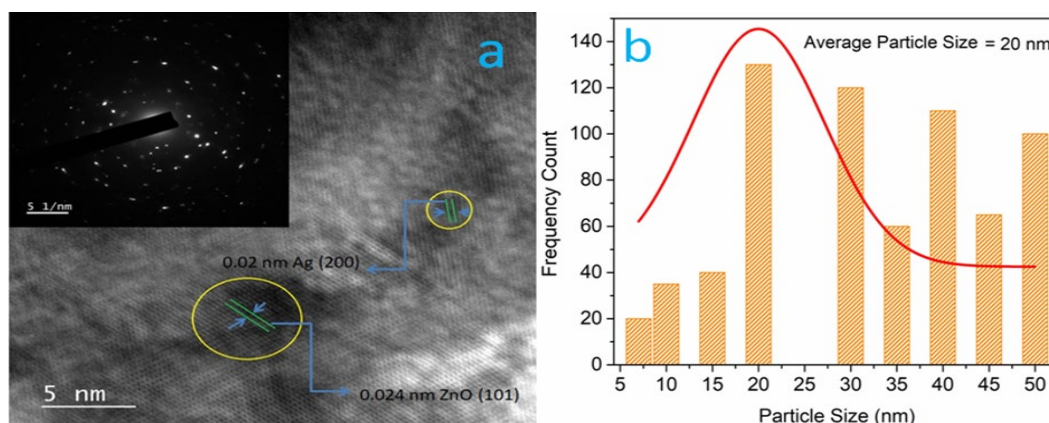


Fig. 6. (a) HRTEM image of Ag doped ZnO NPs (inset shows SAED pattern) and (b) particle size-distribution histogram.

The HRTEM image in Fig. 6 (a) confirmed the distribution of Ag on the ZnO lattice. The (101) plane of ZnO was found to have an interplanar lattice spacing ( $d$ ) of 0.024 nm, while the (200) plane of silver was found to have  $d$  value of 0.02 nm. The XRD investigation also revealed these planes. The polycrystalline nature of the Ag-doped ZnO NPs was demonstrated by the selected area electron diffraction (SAED) pattern of the Ag-doped ZnO NPs, which is displayed inset of Fig. 6(a). It clearly showed the random scattering of diffraction spots coupled with a ring pattern.

### 3.4. FTIR analysis

The FTIR spectra of the active biomolecules from the leaf extract of *Datura metel* L., which served as a capping and reducing agent during the biosynthesis of Ag-doped ZnO nanoparticles, are displayed in Figure 7. The O-H stretching associated with the absorption peak at  $3361\text{ cm}^{-1}$  indicates the presence of flavonoids, tannins, and saponins in the leaf extract of *Datura metel* L. [22]. C = C stretching in the aromatic ring of polyphenols and aliphatic amines was the source of the peaks seen at  $1555$ ,  $1402$ , and  $1017\text{ cm}^{-1}$  [23]. The amine's N-H bending vibration was responsible for the peak at  $833\text{ cm}^{-1}$  [22]. The peak at  $656\text{ cm}^{-1}$  represented the metal oxide characteristics of the Zn-O stretching vibration [24]. The peak at  $552\text{ cm}^{-1}$  was the indicative of Ag doping in to ZnO host lattice [25]. FTIR analysis revealed that in addition to phytochemicals like flavonoids, tannins, saponins, polyphenols, and aliphatic amines, the functional groups found in the biomolecules of *Datura metel* L. leaf extract might also serve as reducing and capping agents for the formation of Ag-doped ZnO nanoparticles and prevent the agglomeration of the nanoparticles in the aqueous extract medium.

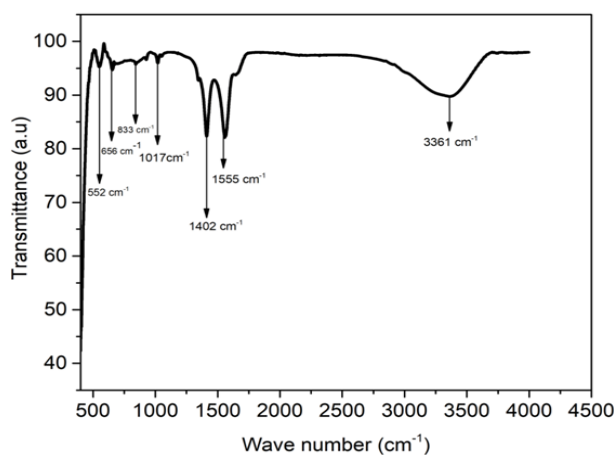


Fig. 7. FTIR spectrum synthesized Ag doped ZnO NPs.

### 3.5. Isolation and identification of microorganisms

Out of 15 isolates that were obtained, based on their morphology, seven isolates—T2, T4, B1, B3, C1, C2, and Ba2—were chosen for additional examination. T4 isolated from spoiled tomato was identified as *Kerstersia gyiorum*, B1 and B3 isolated from spoiled brinjal were identified as *Bacillus altitudinis* and *Klebsiella pneumoniae*, respectively, and C1 and C2 isolated from spoiled chili were identified as *Mammaliococcus sciuri* and *Enterobacter* sp., respectively. These findings were based on the colony morphology on nutrient agar and the 16srRNA sequencing report of the isolates, T2 and Ba2, isolated from spoiled tomato and banana, were identified as *Bacillus subtilis*. Numerous bacteria that could be responsible for the spoiling were found in the spoiled fruit and vegetable samples that were subjected to microbiological analysis in this investigation. Additionally, research suggests that the various types of bacteria may interact intricately and contribute to the spoiling process. Furthermore, there have been reports of fruits and vegetables becoming contaminated with pathogenic microbial strains. Jonathan et al [26] studied the biocontrol efficacy of a group of rhizobacteria, actinomycetes and *Pasteuria penetrans* against *Meloidogyne incognita*, responsible for root-gall in tomato and banana and observed that all the studied microbes enhanced the plant growth for both crops and suppressed root gall development. *Bacillus* sp. have been isolated and identified from healthy and spoiled tomato plants and their rhizosphere and aerial part of the plant as well. Isolation of *Bacillus* sp. from spoiled tomatoes has been reported [27][28][29]. However, these bacteria are widely used in agriculture to stimulate plant growth and development and enhance the defense mechanisms of the plants [30][31]. Strains of *Bacillus* spp. showed antifungal properties against *Alternaria* sp. and *Fusarium* sp. responsible for causing *fusarium* wilt in plants [32][33][34][35]. Sun et al [34] investigated the antagonistic properties of *Bacillus subtilis* against *fusarium* wilt disease in banana and observed inhibition of mycelial growth of *Fusarium* and enhanced the activity of defense related enzymes. *Klebsiella pneumoniae* has been isolated and identified from eggplant fields and are found to be efficient in phosphate solubilization [36][37]. Furthermore, plant pathogenic *Klebsiella pneumonia* has been isolated from brinjal and pomegranate where it caused bark necrosis and wilt [38][39]. However, it has not been linked to its spoilage in brinjal before *Kerstersia gyiorum* is a rare human pathogen, associated with wound infections, neuro-generative diseases and urinary tract infection, and was most probably a contamination from human activity [40][41][42]. Strains of *Bacillus* spp. and *Enterobacter* spp. have been reportedly isolated from fresh chili samples [43]. Members of Enterobacteriaceae family were isolated from chili powder derived from *Capsicum annum* L [44]. *Enterobacter* sp., *Klebsiella* sp., *Pseudomonas* sp., and *Bacillus* sp. evidently caused soft rot in chili pepper [31]. *Enterobacter cloacae*, an opportunistic human pathogen was reported to cause bulb decay in garlic plants and causes diseases such as leaf spots in chili peppers (*Capsicum annum*) [45][46].

### 3.6. Evaluation of the minimum inhibitory concentration

The MIC was determined to quantitatively compare the antimicrobial efficacy of the Ag doped ZnO nanoparticles. The MIC of the samples is listed in Table 2. According to the HG/ T3794-2005 standard, for inorganic antimicrobials, an MIC less than 800 mg/L is identified as qualified [47]. From the table 2 it can be observed that the MICs of the Ag doped ZnO nanoparticles capped with 10 ml *Datura metel* L. leaf extract against *Bacillus altitudinis* and *Klebsiella pneumonia* from spoiled brinjal, *Kerstersia gyiorum* from spoiled tomato and *Bacillus subtilis* from spoiled banana, *Enterobacter* sp. and *Mammaliococcus sciuri* from spoiled chilli, and Ag doped ZnO nanoparticles capped with 40 ml *Datura metel* L. leaf extract against *Bacillus subtilis* isolated from spoiled banana and *Mammaliococcus sciuri* from spoiled chili were much lower than 800 mg/L. From the MIC reports, it was observed that the Ag doped ZnO nanoparticles was more efficient against gram positive bacteria and was in accordance with the results of the antimicrobial activity by agar well diffusion. Similar findings were reported by Amornpitoksuk et al[48] and Adriana et al [49]. Gram-positive and gram-negative bacteria have different cell surfaces, which can be explained by variation in their chemical and structural properties. Compared to gram-negative bacteria, gram-positive bacteria have a significantly simpler cell membrane structure [50]. Moreover, the plasmonic effect of metallic silver and the photoactive ZnO may both be important for the antibacterial activity [49]. Additionally, the antibacterial activity of the nanocomposites is also significantly influenced by their size and the dispersion media [49][51].

### 3.7. Antimicrobial activity

Green synthesized Ag-doped ZnO NPs were tested against three Gram-negative bacteria (*Klebsiella pneumonia*, *Kerstersia gyiorum*, and *Enterobacter sp.*) and four Gram-positive bacteria (*Bacillus subtilis*, *Bacillus altitudinis*, *Mammaliicoccus sciuri*, and *Bacillus subtilis*) isolated from spoiled banana, tomato, brinjal, and chili. For spherical-shaped Ag-doped ZnO NPs (obtained by using 10 ml extract of *Datura metel* L. leaf) and rod-shaped Ag-doped ZnO NPs (obtained by using 40 ml extract of *Datura metel* L. leaf) at the same concentration of 20 mg/L, the zone of inhibition was observed for both Gram-positive and Gram-negative bacteria with varying diameters (Table 3). Spherically shaped Ag-doped ZnO NPs performed better than rod-shaped Ag-doped ZnO NPs in terms of their inhibitory activity value against both Gram-positive and Gram-negative bacteria (Table 3). The variation in NPs' antibacterial activity can be explained by differences in their size, shape, and surface area. Spherical NPs distort the bacterial cell wall more than rod-shaped NPs because of their larger surface area [52]. Furthermore, at a concentration of 20 mg/L, the antibacterial activity of spherically shaped Ag-doped ZnO NPs against both Gram-positive and Gram-negative bacterial isolates was shown to be very close to or considerably higher than that of the conventional antibiotics. Ag-doped ZnO NPs also demonstrated superior antibacterial action against Gram-positive compared to Gram-negative bacterial strains. The variations in the morphological constitutions of Gram-positive and Gram-negative bacteria could possibly be the cause for the difference in sensitivity. Because gram-negative bacteria have an exterior lipopolysaccharide barrier, antimicrobial chemicals cannot pass through their cell walls. Gram-positive bacteria, however, are more vulnerable because they only have an exterior layer of peptidoglycan, which is ineffective as a permeability barrier. Because of this, Gram-negative bacteria have more complex laid out cell walls than Gram-positive bacteria, which serves as a diffusion barrier and reduces their susceptibility to antibacterial drugs [53]. The present findings are consistent with studies from other researchers who performed experiments with different ZnO and Ag-doped ZnO NPs based on plant leaf extracts [54][55][56].

Table 2. MIC of Ag doped ZnO NPs.

Microorganisms	MIC (mg/L)	
	Spherical shaped Ag doped ZnO NPs	Rod shaped Ag doped ZnO NPs
<i>Bacillus subtilis</i>	15	20
<i>Bacillus altitudinis</i>	20	18
<i>Mammaliicoccus sciuri</i>	15	20
<i>Bacillus subtilis</i>	15	15
<i>Klebsiella pneumonia</i>	20	18
<i>Kerstersia gyiorum</i>	20	20
<i>Enterobacter sp.</i>	20	20

Table 3. Zone of inhibition of Ag doped ZnO nanoparticles.

Microorganisms (source)	Zone of Inhibition (mm)							
	Sample A (20 mg/L)	Sample D (20 mg/L)	NIT (300 mcg)	VA (30 mcg)	AMC (30 mcg)	GEN (10 mcg)	CIP (5 mcg)	E (15 mcg)
<b>Gram positive isolates</b>								
<i>Bacillus subtilis</i> (Tomato)	27	14	18	19	14	20	22	20
<i>Bacillus altitudinis</i> (Brinjal)	25	13	20	21	26	26	25	24
<i>Mammaliicoccus sciuri</i> (Chili)	23	10	17	15	12	22	20	20
<i>Bacillus subtilis</i> (Banana)	26	17	21	21	17	15	23	21
<b>Gram negative isolates</b>								
<i>Klebsiella pneumonia</i> (Brinjal)	22	10	12	17	17	12	16	10
<i>Kerstersia gyiorum</i> (Tomato)	20	10	13	14	18	18	15	15
<i>Enterobacter sp.</i> (Chili)	19	10	17	18	17	12	12	18

Nitrofurantoin- [NIT], Vancomycin- [VA], Amoxicillin and clavulanic acid -[AMC], Gentamicin- [GEN], Ciprofloxacin -[CIP], Erythromycin-[E]

### 3.8. Antimicrobial mechanism of Ag doped ZnO NPs

Through a number of ways, the Ag-doped ZnO nanoparticles attack and lyse cells. First, when nanoparticles interact with bacterial cells, the cell membrane gets damaged by changes in membrane protein and enzyme activity, which results in membrane penetration [57]. As a result, Ag and ZnO nanoparticles can enter the bacterial cell, and the membrane protein and lipid bilayer are defaced. This in turn develops an imbalance within the cell and as a result there is cell death. Second, the Ag doped ZnO nanoparticles' surface oxidation releases  $Ag^+$ , which affects the electrostatic interactions between the ions and the negatively charged bacterial cell wall. Third, once the nanoparticles enter the bacterial cell, cytoplasm starts to trickle out, which causes the cell membrane to shrink and the bacteria to die [58]. Fourth, Ag-doped ZnO nanoparticles prevent DNA replication by releasing  $Ag^+$ , which interacts with sugar-phosphate groups to produce gene mutations and alter bacterial cellular activity[58][59]. Last but not least, essential cell processes including DNA replication, transcription, and translation are stopped when ZnO nanoparticles or the reactive oxygen species (ROS) they generate block the signal transduction pathway, leading to cell death [22]. Ag-doped ZnO nanoparticles' antibacterial mechanism is schematically illustrated in Figure 8.

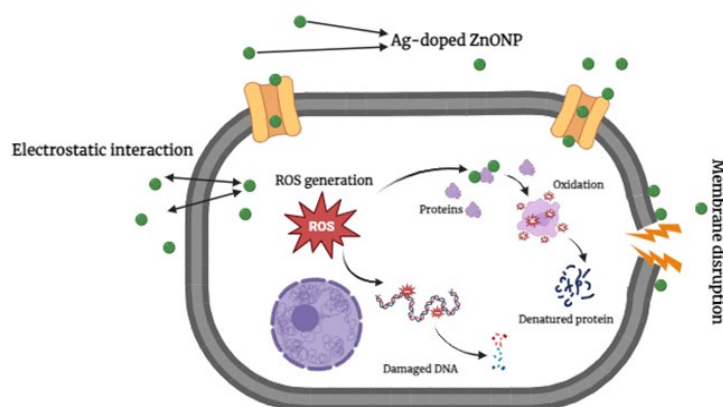


Fig. 8. Schematic illustration of antimicrobial mechanism of Ag doped ZnO nanoparticles.

#### 4. Conclusion

*Datura metel* L. leaf extract has been successfully employed as a reducing and capping agent in the preparation of Ag doped ZnO NPs employing a unique green synthesis technique. EDAX, TEM, HRTEM, FESEM, and XRD were used to characterize the produced Ag doped ZnO NPs. XRD, EDAX, TEM, and HRTEM confirmed that Ag-doped ZnO NPs were formed. It was clear from the FESEM analysis that the volume of *Datura metel* L. leaf extract affected the shape of Ag-doped ZnO NPs. FTIR was used to determine the functional groups that were present in the leaf extract of *Datura metel* L. The antibacterial activity of Ag-doped ZnO were tested against Gram-negative and Gram-positive bacteria that were isolated from banana, tomato, brinjal, and chili.

Ag-doped ZnO NPs were found to exhibit significant antibacterial properties against both Gram-positive and Gram-negative bacteria. In contrast to Gram-negative bacteria, the produced NPs demonstrated more potency against Gram-positive bacteria. Because of their combined biocompatibility and excellent microbial activity, it is expected that Ag-doped ZnO NPs synthesized with leaf extract from *Datura metel* L. will be more effective against microorganisms. By using this method, these nanoparticles may help in the development of an antibacterial drug that would stop post-harvest losses of fruits and vegetables caused by microbes.

#### Acknowledgements

This work was financially supported by Department of Biotechnology (DBT), Government of India (project file no. BT/NER/143/SP44474/2021).

#### References

- [1] I. K. Arah, H. Amaglo, E. K. Kumah, H. Ofori, *Int. J. Agron.*, 2015(1), 478041, (2015); <https://doi.org/10.1155/2015/478041>
- [2] K. V Sucharitha, A. M. Beulah, K. Ravikiran, *Int. Food Res. J.*, 25(1), 93-99, (2018).
- [3] I. Domínguez, F. Ferreres, F. P. del Riquelme, R. Font, M. I. Gil, *Postharvest Biol. Technol.*, 72, 1-10, (2012); <https://doi.org/10.1016/j.postharvbio.2012.04.010>
- [4] M. Meena et al., *Sci. Rep.*, 10(1), 21914, (2020); <https://doi.org/10.1038/s41598-020-78924-9>
- [5] J. G. de Oliveira Filho, M. Miranda, M. D. Ferreira, A. Plotto, *Foods*, 10(10), 2438, (2021); <https://doi.org/10.3390/foods10102438>
- [6] V. Jagadeeswar, V. Dhinesh, S. M. Roopan, E. J. J. Samuel, *Colloid J.*, 85(5), 827-845, (2023); <https://doi.org/10.1134/S1061933X23600513>

- [7] F. Habtamu, S. Berhanu, and T. Mender, *J. Chem.*, 2021(1), 2451836, (2021); <https://doi.org/10.1155/2021/2451836>
- [8] D. S. Dutta, M. K. Kalita, P. D. Nath, *J. Environ. Biol.*, 43(3), 460-467, (2022); <https://doi.org/10.22438/jeb/43/3/MRN-2002>
- [9] K. C. Ukkund, M. P. Patil, M. B. Madalageri, R. M. Ravindra Mulage, R. C. Jagadeesh, *Karnataka Journal of Agricultural Sciences*, 20(1),99-101 (2007).
- [10] N. J. Swagato, N. Parvin, S. Ahsan, M. S. Kabir, *Int. Food Res. J.*,22(4), (2015).
- [11] R. Martí, S. Roselló, J. Cebolla-Cornejo, *Cancers (Basel)*., 8(6),58, (2016); <https://doi.org/10.3390/cancers8060058>
- [12] P. Basumatary, S. Dutta, M. K. Bhuyan, M. Neog, *Indian J. Hill Farming*, 35, no. Spcl, 129-133, (2022)
- [13] P. K. Khatri, S. Sharma, *Int. J. Curr. Microbiol. Appl. Sci.*, 7(12), 2671-2679, (2018); <https://doi.org/10.20546/ijcmas.2018.712.303>
- [14] N. A. Hasan, I. M. Zulkahar, AIP Publishing, 2020 (1); <https://doi.org/10.1063/1.5062699>
- [15] D. F. George et al., *Int. Sch. Res. Not.*, 2012(1), 658470, (2012); <https://doi.org/10.5402/2012/658470>
- [16] K. A. A. A. Rahim, A. M. A. Mohamed, *Jundishapur J. Microbiol.*, 7(11), (2014); <https://doi.org/10.5812/jjm.17114>
- [17] M. J. Klink, N. Laloo, A. Leudjo Taka, V. E. Pakade, M. E. Monapathi, J. S. Modise, *Molecules*, 27(11), 3532, (2022); <https://doi.org/10.3390/molecules27113532>
- [18] T. Iqbal, A. Raza, M. Zafar, S. Afsheen, I. Kebaili, H. Alrobei, *Appl. Nanosci.*, 12, 1-13, (2022); <https://doi.org/10.1007/s13204-021-02238-z>
- [19] M. S. Mthana, M. N. Mthiyane, A. C. Ekennia, M. Singh, D. C. Onwudiwe, *Sci. African*, 17, e01365, (2022); <https://doi.org/10.1016/j.sciaf.2022.e01365>
- [20] R. Kumar, G. Ghoshal, A. Jain, M. Goyal, *J. Nanomed. Nanotechnol.*, 8(4), 1-8, (2017); <https://doi.org/10.4172/2157-7439.1000452>
- [21] J. Jalab, W. Abdelwahed, A. Kitaz, R. Al-Kayali, *Heliyon*, 7(9), (2021); <https://doi.org/10.1016/j.heliyon.2021.e08033>
- [22] S. G. Mtavangu, R. L. Machunda, B. van der Bruggen, K. N. Njau, *Sci. Rep.*, 12(1), 15359, (2022); <https://doi.org/10.1038/s41598-022-19403-1>
- [23] F. Rahman et al., *R. Soc. Open Sci.*, 9(11), 220858, (2022); <https://doi.org/10.1098/rsos.220858>
- [24] P. Ramesh, K. Saravanan, P. Manogar, J. Johnson, E. Vinoth, M. Mayakannan, *Sens. Bio-Sensing Res.*, 31, 100399, (2021); <https://doi.org/10.1016/j.sbsr.2021.100399>
- [25] S. Gayathri et al., *Materials Chemistry and Physics*, 167, 194-200, (2015). <https://doi.org/10.1016/j.matchemphys.2015.10.031>
- [26] E. I. Jonathan, K. R. Barker, F. F. Abdel-Alim, T. C. Vrain, D. W. Dickson, *Nematropica*., 30 231-240, (2000).
- [27] M. Barth, T. R. Hankinson, H. Zhuang, F. Breidt, *Compend. Microbiol. spoilage foods beverages*, 135-183, (2009); [https://doi.org/10.1007/978-1-4419-0826-1\\_6](https://doi.org/10.1007/978-1-4419-0826-1_6)
- [28] B. Thiyam, G. D. Sharma, *Curr. World Environ.*, 8(2),319-322, (2013); <https://doi.org/10.12944/CWE.8.2.20>
- [29] D. Singh, R. R. Sharma, *Postharvest disinfection of fruits and vegetables*, Elsevier, 2018, 1-52(2018); <https://doi.org/10.1016/B978-0-12-812698-1.00001-7>
- [30] A. I. O. Jideani, H. Silungwe, T. Takalani, A. O. Omolola, H. O. Udeh, T. A. Anyasi, *Int. J. Food Prop.*, 24(1), 41-67, (2021); <https://doi.org/10.1080/10942912.2020.1866597>
- [31] A. Partoazar, S. Afrasiabi, F. Ghasemzadeh, M. Ghazi-Khansari, M. M. S. Dallal, *Bionanoscience*, 13(4),2096-2102, (2023); <https://doi.org/10.1007/s12668-023-01165-3>
- [32] F. Y. O. Rocha, C. M. de Oliveira, P. R. A. da Silva, L. H. V. de Melo, M. G. F. do Carmo, J. I. Baldani, *Appl. soil Ecol.*, 120, 8-19, (2017); <https://doi.org/10.1016/j.apsoil.2017.07.025>

- [33] V. Shanmugam, K. Atri, S. Gupta, N. Kanoujia, D. S. Naruka, *Folia Microbiol. (Praha)*, 56, 170-177, (2011); <https://doi.org/10.1007/s12223-011-0031-3>
- [34] J. B. Sun, M. Peng, Y. G. Wang, P. J. Zhao, Q. Y. Xia, *African J. Microbiol. Res.*, 5(5), 509-515, (2011)
- [35] P. S. de O. Nunes, F. H. V De Medeiros, T. S. De Oliveira, J. R. de Almeida Zago, W. Bettiol, *Brazilian J. Microbiol.*, 54(1), 397-406, (2023); <https://doi.org/10.1007/s42770-022-00874-3>
- [36] K. Sungthongwises, M. Matsuoka, K. Ohnishi, S. Tanaka, C. B. Iwai, II International Symposium on Horticulture in Europe 1099, 333-337, (2012).
- [37] S. R. Das et al., *Arch. Microbiol.*, 204(3), 199, (2022); <https://doi.org/10.1007/s00203-022-02809-w>
- [38] T. S. Ajayasree, S. G. Borkar, *J. Appl. Biotechnol. Bioeng.*, 5(6), 329-332, (2018); <https://doi.org/10.15406/jabb.2018.05.00159>
- [39] I. F. Ossamulu, H. O. Akanya, E. C. Egwim, A. Y. Kabiru, *Journal of Science, Technology, Mathematics and Education (JOSTMED)*.17(1), 55-67, (2021).
- [40] Y. Ogawa et al., *J. Infect. Chemother.*, 22(4), 265-267, (2016); <https://doi.org/10.1016/j.jiac.2015.11.003>
- [41] M. A. Pence, J. Sharon, E. McElvania Tekippe, B. L. Pakalniskis, B. A. Ford, C.-A. D. Burnham, *J. Clin. Microbiol.*, 51(6), 2001-2004, (2013); <https://doi.org/10.1128/JCM.00829-13>
- [42] I. Baran, A. P. Düzgün, İ. Mumcuoğlu, N. Aksu, *BMC Infect. Dis.*, 17, 1-8, (2017); <https://doi.org/10.1186/s12879-017-2711-3>
- [43] N. A. Nafady, S. A. M. Alamri, E. A. Hassan, M. Hashem, Y. S. Mostafa, K. A. M. Abo-Elyousr, *Folia Hortic.*, 31(2), 319-329, (2019); <https://doi.org/10.2478/fhort-2019-0025>
- [44] Y. F. Hernández Gómez et al., *Microorganisms*, 10(8), 1677, (2022); <https://doi.org/10.3390/microorganisms10081677>
- [45] E. F. Li, X. L. Tian, R. B. Zhao, Y. H. Wang, G. Wang, *Plant Dis.*, 106(1), 310, (2022); <https://doi.org/10.1094/PDIS-05-21-0972-PDN>
- [46] P. L. Babu, D. Singh, J. Rajender, N. Geat, R. Patidar, *New Dis. Reports*, 48(2), 10-11, (2023); <https://doi.org/10.1002/ndr2.12225>
- [47] Y. Hou, J. Feng, Y. Wang, L. Li, *J. Mater. Sci. Mater. Electron.*, 27, 6615-6622, (2016); <https://doi.org/10.1007/s10854-016-4669-0>
- [48] P. Amornpitoksuk, S. Suwanboon, S. Sangkanu, A. Sukhoom, N. Muensit, *J. Baltrusaitis, Powder Technol.*, 219, 158-164, (2012); <https://doi.org/10.1016/j.powtec.2011.12.032>
- [49] A. B. P. Jiménez, C. A. H. Aguilar, J. M. V. Ramos, P. Thangarasu, *Aust. J. Chem.*, 68(2), 288-297, (2014); <https://doi.org/10.1071/CH14123>
- [50] C. Abinaya et al., *Mater. Chem. Phys.*, 184, 172-182, (2016); <https://doi.org/10.1016/j.matchemphys.2016.09.039>
- [51] A. Khan et al., *Spectrochim. Acta Part A Mol. Biomol. Spectrosc.*, 290, 122296, (2023); <https://doi.org/10.1016/j.saa.2022.122296>
- [52] S. Getie, A. Belay, A. R. Chandra Reddy, Z. Belay, *J Nanomed Nanotechnol*, 8(004), (2017); <https://doi.org/10.4172/2157-7439.S8-004>
- [53] K. Arora, *J. Chem. Pharm. Res.*, 7(12), 91-95, (2015).
- [54] S. Vijayakumar, B. Vaseeharan, B. Malaikozhundan, M. Shobiya, *Biomed. Pharmacother.*, 84, 1213-1222, (2016); <https://doi.org/10.1016/j.biopha.2016.10.038>
- [55] S. Jabeen, *J. Water Environ. Nanotechnol.*, 5(4), 307-320, (2020).
- [56] D. Acharya, K. M. Singha, P. Pandey, B. Mohanta, J. Rajkumari, L. P. Singha, *Sci. Rep.*, 8(1), 201, (2018); <https://doi.org/10.1038/s41598-017-18590-6>
- [57] N. Padmavathy, R. Vijayaraghavan, *J. Biomed. Nanotechnol.*, 7(6), 813-822, (2011); <https://doi.org/10.1166/jbn.2011.1343>

- [58] I. Matai, A. Sachdev, P. Dubey, S. U. Kumar, B. Bhushan, P. Gopinath, Colloids Surfaces B Biointerfaces, 115, 359-367, (2014); <https://doi.org/10.1016/j.colsurfb.2013.12.005>
- [59] M. K. Rai, S. D. Deshmukh, A. P. Ingle, A. K. Gade, J. Appl. Microbiol., 112(5), 841-852, (2012); <https://doi.org/10.1111/j.1365-2672.2012.05253.x>